Primakoff production of π^0, η, and η' in the Coulomb field of a nucleus

Murat M. Kaskulov* and Ulrich Mosel
Institut für Theoretische Physik, Universität Giessen, D-35392 Giessen, Germany
(Received 31 March 2011; revised manuscript received 18 August 2011; published 27 December 2011)

Photoproduction of neutral pseudoscalar mesons π^0, $\eta(547)$, and $\eta'(958)$ in the Coulomb field of an atomic nucleus is studied using a model which describes the Primakoff and nuclear parts of the production amplitude. At high energies the nuclear background is dominated by the exchange of C-parity odd Regge trajectories. In the coherent production the isospin filtering makes the $\omega(782)$ a dominant trajectory. The calculations are in agreement with π^0 data from JLAB provided the photon shadowing and final state interactions of mesons are taken into account. The kinematic conditions which allow to study the Primakoff effect in η and η' photoproduction off nuclei are further discussed. We also give predictions for the higher energies available at the JLAB upgrade.

DOI: 10.1103/PhysRevC.84.065206 PACS number(s): 25.20.Lj, 11.80.La, 13.60.Le, 14.20.Dh

I. INTRODUCTION

The coherent photoproduction of neutral pions

$$\gamma + A \to \pi^0 + A$$

in the Coulomb field of a nucleus was first discussed by Primakoff [1] as a plausible way to measure the π^0 lifetime. Indeed, at high energies the Coulomb $\gamma\gamma^* \to \pi^0$ component gets well separated from the background induced by nuclear interactions and shows up as a resonant peak in the angular distributions at forward angles—the Primakoff effect. A conversion of photons into particles in the Coulomb field is remarkably general and can dominate in many other reactions where the nucleus stays in its ground state after the scattering. The Primakoff effect has been observed in the high energy reactions involving the hadronic probes where it was used to measure the radiative decay widths of mesons and baryons. The most important applications of the Primakoff process are the measurements of radiative life times of vector $\rho^{\pm}(770)$ [2–5], $K^{*\pm}(890)$ [6–8], and axial-vector $a_1(1260)$ [9], $b_1(1235)$ [10] mesons in the coherent high energy $\pi(K) \to$ meson excitation on nuclear targets. The measurement of the Λ to $\gamma\Sigma^0$ transition is another well-known example [11,12]. Presently the Primakoff effect is an important experimental tool to study the physics beyond the standard model. For instance, the hypothetical axions being produced in the Sun via the Primakoff process are presently searched for using the inverse effect in the CAST experiment at CERN [13]. The Primakoff physics will be studied from new perspectives with an upgrade of JLAB to 12 GeV and at the COMPASS detector at CERN where many reaction channels involving vector, axial-vector, and hybrid mesons will be investigated in the near future.

High energy photoproduction of pseudoscalar mesons $\pi^0(134)$, $\eta(547)$, and $\eta'(958)$ studied in the present work is of special interest. The two-photon decay widths of these mesons are determined by the axial anomaly in QCD [14,15]. Therefore, based on the original proposal [1] the production reactions off nuclei provide a tool to measure these quantities. This has been followed in [16–19] where the $\pi^0 \to \gamma\gamma$ and $\eta \to \gamma\gamma$ decay widths were measured. Presently a new generation of experiments [20] allows to measure the $\pi^0 \to \gamma\gamma$ decay width via the Primakoff effect on a few percent level. Also high precision η and η' experiments are planned at JLAB [21].

However, any experimental determination of the radiative decay widths of mesons via the Primakoff effect on nuclei has to deal with the presence of nuclear production processes. Theoretically, it is important to control the reaction mechanisms in close vicinity of the Coulomb peak. This is because the Primakoff production is contaminated by events which come from the coherent and incoherent conversions in the strong field of a nucleus. Moreover, the nuclear coherent amplitudes introduce complex phases and by interference with the Primakoff amplitude affect the $\gamma\gamma^* \to$ meson signal. In some cases these two mechanisms can be well separated. For instance, at very high energies the growth of the Coulomb peak must dominate over the Regge behavior of the strong amplitude. However, both amplitudes necessarily interfere which makes the interpretation of the results model dependent. The strong part of the amplitude is of much shorter range and the nuclear conversion happens predominantly deep inside the nucleus. Therefore, the fate of particles in the initial and final state interactions have to be taken into account. All together these require a model which properly deals with the nuclear background, both coherent and incoherent, and describes the data on the same level of accuracy as required by the experiment.

There are well-formulated procedures to calculate the incoherent pion photoproduction cross sections using, e.g., the transport [22], cascade [23], or Glauber [24,25] methods. Morpurgo [26] and Fäldt [27] have laid the theoretical basis for the treatment of the Primakoff effect on nuclei. Both had to assume simplified expressions for the elementary strong production amplitude. Also in the more recent approach [28] which investigates final and initial state interactions, the elementary amplitudes were parametrized without any detailed comparison to experimental data on the nucleon. A recent experimental analysis [20] has shown that agreement with experiment could only be reached if additional parameters fixing the relative strength and phase of the Primakoff and the

*murat.kaskulov@theo.physik.uni-giessen.de

nuclear coherent amplitudes from [28] were introduced; these parameters even depended on target-mass number.

In this work we, therefore, develop a model for the high energy coherent production of pseudoscalar mesons off nuclei. Starting from the high energy production off nucleons, we show, that from the photon (γ) and Regge exchange perspectives both the nuclear Primakoff and strong amplitudes can be well described using the same general expressions for both components and no free parameters such as relative strengths and phases. We further investigate the impact of initial and final state interactions on the reaction cross section.

The use of tagged photon beams at JLAB will allow to access $\eta \to \gamma\gamma$ and $\eta' \to \gamma\gamma$ decay widths in the Primakoff production off nuclei [21]. We therefore consider also the coherent photoproduction of η and η' and study the kinematic conditions which allow to separate the Primakoff peak from the nuclear background interactions.

This work is organized as follows. In Sec. II we discuss the radiative decays of pseudoscalar and vector mesons in the vector dominance model. Photoproduction of π^0, η and η' mesons off nucleons with transition amplitudes derived in Sec. II is considered in Sec. III. In Sec. IV we propose a model for the high energy coherent production of pseudoscalar mesons off nuclei. The results are presented in Sec. V. The summary is given in Sec. VI.

II. PRELIMINARIES

The radiative $\gamma\gamma$ decay widths of neutral pseudoscalar mesons $P = \pi^0$, η, and η' measured in the Primakoff process off nuclei are tied to the description of the strong nuclear background. The latter is dominated (at high energies) by the exchange of vector mesons (V) which interact via the anomalous $V\gamma \to P$ transitions. Furthermore, at high energies the hadronic $\gamma \leftrightarrow V$ components of the photon in $P \to \gamma\gamma$ and $P \to VV$ transitions have to be taken into account explicitly. In the nuclear medium this effect is known as shadowing, i.e., a photon behaves in strong interactions like a hadron [29]. In this section we attempt to formalize these features relevant for the present work in a common framework.

The decays of pseudoscalar mesons $\pi^0 \to \gamma\gamma$, $\eta \to \gamma\gamma$, and $\eta' \to \gamma\gamma$ are described (at leading order) by the Wess-Zumino-Witten (WZW) term [30,31], which accounts for the anomalies in the framework of an effective theory. The corrections to the WZW term concern $\eta - \eta'$ mixing. In a theory which accommodates the mixing pattern of $\eta - \eta'$ mesons a decent approximation to all three decays can be obtained [32]. On the other hand, a common description of the anomalous $P \to \gamma\gamma$, $P \to VV$, and $P \to V\gamma$ interactions and $\gamma \to V$ transition, where V includes the $\rho^0(770)$, $\omega(782)$, and $\phi(1020)$ vector mesons, can be realized using the vector dominance model (VDM), see [33] and references therein. The corresponding VDM diagrams are shown in Fig. 1.

The anomalous VVP interaction followed here reads

$$\mathcal{L}_{VVP} = -\frac{N_c g^2}{32\pi^2 f_0}\varepsilon^{\mu\nu\alpha\beta}\langle \partial_\mu V_\nu \partial_\alpha V_\beta P\rangle, \tag{1}$$

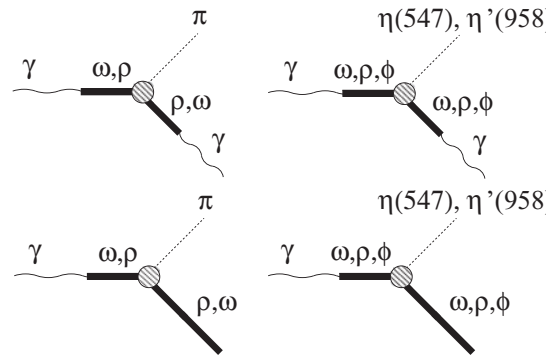

FIG. 1. Diagrams describing the anomalous $\gamma + \gamma(V) \to \pi^0$, $\eta(547)$, and $\eta'(958)$ transition in VDM. Vector mesons V include $\rho(770)$, $\omega(782)$, and $\phi(1020)$ states.

where P and V_μ describe the nonet of pseudoscalar mesons and nonet of vector mesons, respectively (see the Appendix). In Eq. (1) $\varepsilon^{\mu\nu\alpha\beta}$ denotes the totally antisymmetric Levi-Civita tensor, f_0 is normalized to the pion decay constant $f_\pi \simeq 92.4$ MeV and $N_c = 3$ stands for the number of quark colors. The coupling of the electromagnetic field $\mathcal{A}$ to the vector mesons is given by [33,34]

$$\mathcal{L}_{\gamma V} = e\frac{m_V^2}{g}\mathcal{A}^\mu \langle Q V_\mu\rangle, \tag{2}$$

where $Q = \mathrm{diag}(2/3, -1/3, -1/3)$ is a quark charge matrix and $e \simeq -\sqrt{4\pi/137}$.

Working out the traces $\langle \ldots \rangle$ the VDM takes the form

$$\begin{aligned}\mathcal{L}_{VVP} = -\frac{N_c g^2}{8\pi^2 f_\pi}\varepsilon^{\mu\nu\alpha\beta}\Bigg[&\partial_\mu\rho_\nu^0\partial_\alpha\omega_\beta\pi^0 \\ &+ \left(\partial_\mu\rho_\nu^0\partial_\alpha\rho_\beta^0 + \partial_\mu\omega_\nu\partial_\alpha\omega_\beta\right)\left[\frac{\eta_8}{2\sqrt{3}} + \frac{\eta_0}{\sqrt{6}}\right] \\ &+ \partial_\mu\varphi_\nu\partial_\alpha\varphi_\beta\left[\frac{-\eta_8}{\sqrt{3}} + \frac{\eta_0}{\sqrt{6}}\right]\Bigg] + \cdots,\end{aligned} \tag{3}$$

$$\mathcal{L}_{\gamma V} = e\frac{m_V^2}{g}\left[\rho_\mu^0 + \frac{1}{3}\omega_\mu - \frac{\sqrt{2}}{3}\phi_\mu\right]\mathcal{A}^\mu. \tag{4}$$

In Eq. (3) only the neutral components needed in this work are shown. As usual the observed η and η' eigenstates are the mixtures of the flavor singlet η_0 and octet η_8 states

$$\begin{pmatrix}\eta \\ \eta'\end{pmatrix} = \begin{pmatrix}-\sin\vartheta & \cos\vartheta \\ \cos\vartheta & \sin\vartheta\end{pmatrix}\begin{pmatrix}\eta_0 \\ \eta_8\end{pmatrix}, \tag{5}$$

where ϑ is the $\eta - \eta'$-mixing angle. At this point we do not take the $\pi^0 - \eta - \eta'$ isospin violating mixing into account which may become important for a very accurate determination of the decay widths [35].

In the two-step $P \to VV \to \gamma(q,\lambda)\gamma(q',\lambda')$ decay processes the transition amplitudes are given by

$$-iM_{P\to\gamma\gamma} = \frac{i\alpha}{\pi f_\pi}c_P\varepsilon^{\mu\nu\alpha\beta}q_\mu\epsilon_\nu^{\lambda\dagger}q'_\alpha\epsilon_\beta^{\lambda'\dagger}, \tag{6}$$

where $\alpha = \frac{e^2}{4\pi}$, ϵ^λ is the polarization vector of photons ($\lambda = \pm 1$), $c_{\pi^0} = 1$, $c_\eta = \frac{1}{\sqrt{3}}(\cos\vartheta - 2\sqrt{2}\sin\vartheta)$, and $c_{\eta'} =$

$\frac{1}{\sqrt{3}}(\sin\vartheta + 2\sqrt{2}\cos\vartheta)$. Using Eq. (6) the $\gamma\gamma$ decay widths of neutral pseudoscalars are given by

$$\Gamma_{P\to\gamma\gamma} = \frac{\alpha^2}{64\pi^3 f_\pi^2} m_P^3 c_P^2 \,. \tag{7}$$

The measured values are well described using $\vartheta \simeq -16^\circ$ resulting in $\Gamma_{\pi\to\gamma\gamma} = 7.73$ eV, $\Gamma_{\eta\to\gamma\gamma} = 0.52$ keV and $\Gamma_{\eta'\to\gamma\gamma} = 5.48$ keV. The masses of mesons are [36] $m_{\pi^0} = 134.9$ MeV, $m_\eta = 547.9$ MeV, and $m_{\eta'} = 957.8$ MeV.

The experimental $\gamma\gamma$ decay width of π^0 is [36]

$$\Gamma^{\rm exp}_{\pi^0\to\gamma\gamma} = (7.74 \pm 0.55) \ \text{eV}, \tag{8}$$

as required by the anomaly. Note that the corresponding decay width measured via the Primakoff effect $\Gamma_{\pi^0\to\gamma\gamma} = (7.82 \pm 0.14)$ eV [20] agrees with Eq. (8). However, in the η channel the $\gamma\gamma$ decay width $\Gamma_{\eta\to\gamma\gamma} = (0.32 \pm 0.046)$ keV measured at Cornell [18] when using the Primakoff effect[1] is at variance with the measurements via the QED production in e^+e^- collisions [36] where

$$\Gamma^{\rm exp}_{\eta\to\gamma\gamma} = (0.51 \pm 0.026) \ \text{keV}. \tag{9}$$

As for $\eta' \to \gamma\gamma$ decay the width was measured in the e^+e^- collisions with the value of [36]

$$\Gamma^{\rm exp}_{\eta'\to\gamma\gamma} = (4.28 \pm 0.19) \ \text{keV}. \tag{10}$$

In the Primakoff production one of two photons is off-mass-shell. In VDM the half-off-shell $\gamma(q)\gamma^*(l) \to P(k)$ vertices to be used in the following read

$$-iM^\beta_{\gamma\gamma^*\to P} = \frac{i\alpha}{\pi f_\pi}\varepsilon^{\mu\nu\alpha\beta} q_\mu \epsilon^\lambda_\nu l_\alpha \, F^P_{\gamma\gamma^*}(l^2), \tag{11}$$

where

$$F^\pi_{\gamma\gamma^*}(l^2) = \tfrac{1}{2}[F_\rho(l^2) + F_\omega(l^2)], \tag{12}$$

$$F^\eta_{\gamma\gamma^*}(l^2) = \sqrt{3}\left[\left[F_\rho(l^2) + \frac{1}{9}F_\omega(l^2)\right]\left(\frac{\cos\vartheta}{2} - \frac{\sin\vartheta}{\sqrt{2}}\right) - \frac{2}{9}F_\phi(l^2)\left(\cos\vartheta + \frac{\sin\vartheta}{\sqrt{2}}\right)\right], \tag{13}$$

$$F^{\eta'}_{\gamma\gamma^*}(l^2) = \sqrt{3}\left[\left[F_\rho(l^2) + \frac{1}{9}F_\omega(l^2)\right]\left(\frac{\cos\vartheta}{\sqrt{2}} + \frac{\sin\vartheta}{2}\right) + \frac{2}{9}F_\phi(l^2)\left(\frac{\cos\vartheta}{\sqrt{2}} - \sin\vartheta\right)\right] \tag{14}$$

with VDM (form) factors $F_V(l^2) = \frac{m_V^2}{m_V^2 - l^2 - i0^+}$. For the calculations of form factors in an improved VDM framework see [39].

The transition amplitude $\gamma(q)V(l) \to P(k)$ relevant for our purpose can be derived from the Lagrangian Eq. (3) and from the γV transitions of the nonanomalous Lagrangian Eq. (4). It takes the form

$$-iM_{\gamma V\to P} = -ieG_{\gamma VP}\varepsilon^{\mu\nu\alpha\beta} q_\mu \epsilon^\lambda_\nu l_\alpha \epsilon^{\lambda'(V)}_\beta, \tag{15}$$

where $G_{\gamma VP} = \frac{g}{8\pi^2 f_\pi} b^{\gamma(V)}_{(P)}$, $\epsilon^{\lambda'(V)}$ is the polarization vector of V with $\lambda' = 0, \pm 1$ and the coefficients $b^{\gamma(V)}_{(P)} = b^{\gamma(\rho,\omega,\phi)}_{(\pi,\eta,\eta')}$ are given by

$\gamma\rho$	$\gamma\omega$	$\gamma\phi$	
1	3	0	π
$\sqrt{3}(\cos\vartheta - \sqrt{2}\sin\vartheta)$	$\frac{(\cos\vartheta - \sqrt{2}\sin\vartheta)}{\sqrt{3}}$	$\frac{(2\sqrt{2}\cos\vartheta + 2\sin\vartheta)}{\sqrt{3}}$	η
$\sqrt{3}(\sin\vartheta + \sqrt{2}\cos\vartheta)$	$\frac{(\sin\vartheta + \sqrt{2}\cos\vartheta)}{\sqrt{3}}$	$\frac{(2\sqrt{2}\sin\vartheta - 2\cos\vartheta)}{\sqrt{3}}$	η'

The VDM coupling g is supposed to be universal. The value of $g \simeq 6$ is determined from the $\rho^0 \to \pi^+\pi^-$ decay width $\Gamma_{\rho^0\to\pi^+\pi^-} = \frac{g^2}{48\pi} m_\rho (1 - 4m_\pi^2/m_\rho^2)^{3/2}$ and approximates well the transition rates in Eq. (15). For instance, in the reaction channels $\gamma\rho(\omega) \to \pi^0, \eta, \eta'$ needed in the following the corresponding radiative decay widths $\Gamma_{V\to\gamma P} = \frac{\alpha}{24}\frac{G^2_{\gamma VP}}{m_V^3}(m_V^2 - m_P^2)^3$ and/or $\Gamma_{P\to\gamma V} = \frac{\alpha}{8}\frac{G^2_{\gamma VP}}{m_P^3}(m_P^2 - m_V^2)^3$ calculated using the universality of g and Eq. (15) agree well with [36]. The coupling g will also show up in the interaction of ρ meson with nucleons. In this form the anomalous $\gamma V \to P$ and strong ρNN interactions get correlated reducing largely the number of free parameters.

In the photoproduction of P the vector mesons are exchanged in the t-channel. The corresponding transition vertices which will enter the production amplitude off nucleons and nuclei read

$$-iM^\beta_{\gamma V^*\to P} = -ieG_{\gamma VP}\varepsilon^{\mu\nu\alpha\beta} q_\mu \epsilon^\lambda_\nu l_\alpha. \tag{16}$$

III. PHOTOPRODUCTION OFF NUCLEONS

The production of charged pions off nucleons with high energy real and virtual photons has been studied in [40]. In the neutral π^0 channel the Primakoff effect together with exchanges of C-parity odd vector $\rho(770)$, $\omega(782)$ and axial-vector $b_1(1235)$ and $h_1(1170)$ Regge trajectories has been calculated [41]. As a novel feature the contributions of s- and u-channel nucleon resonances were investigated. The latter were described using the Bloom-Gilman connection between the exclusive and (deep inelastic) inclusive reactions. The resonances are effective in the off-forward region around the diffractive dip and in the deeply virtual (high Q^2) electroproduction where the quarks are the relevant degrees of freedom [42].

At the real photon point the high energy forward production of π^0 is dominated by the t-channel exchange of mesons, with ω and ρ being the dominant Regge trajectories. For the η and η' channels we assume the dominance of these exchange contributions as well. In the model of [40,41] the sum of s- and u-channel contributions cancel at the forward angles. Also the contributions of axial-vector mesons are small and can be readily neglected. A detailed comparison with data on the nucleon has been performed in [40,41]. The dominance

[1] In Ref. [37] $\Gamma_{\eta\to\gamma\gamma}$ has been fitted to the Primakoff effect off protons. The value of $\Gamma_{\eta\to\gamma\gamma}$ from this fit is ~50% bigger than from e^+e^- experiments, Eq. (9). However, the authors of [37] miss the factor e^2 in their expressions for the Primakoff cross section which makes the Coulomb components of [37] and [38] too large by one order of magnitude.

of ω- and ρ-exchanges at forward angles makes the model similar (up to the Regge phase of the ρ-exchange) to that proposed by Laget in [43]. However, contrary to [43] we rely on a VDM framework which resolves the hadronic structure of the anomalous vertex needed in a consistent treatment of shadowing and allows to fix the relative sign between the Primakoff and strong amplitudes. The VDM form factors further introduce an additional t dependence; they become important in the production of heavy η and η' mesons which require sizable momentum transfer to the target already at forward angles.

In the Primakoff production of π^0, η and η' off protons the amplitude takes the form

$$-iT^{\gamma}_{\gamma p\to Pp} = -i|e|\, M^{\mu}_{\gamma\gamma^*\to P}\, D^{\gamma}_{\mu\nu}(l) \times \bar{u}_{s'}(p')\left[F_1^p\gamma^{\nu} - F_2^p\frac{i\sigma^{\nu\sigma}l_{\sigma}}{2m_N}\right]u_s(p), \quad (17)$$

where $l = p - p'$, $D^{\gamma}_{\mu\nu}$ is the photon propagator

$$iD^{\gamma}_{\mu\nu}(l) = \left[-g_{\mu\nu} + \frac{l_{\mu}l_{\nu}}{l^2}\right]\frac{i}{l^2 + i0^+}, \quad (18)$$

and $F_1^p(F_2^p)$ stands for the Dirac (Pauli) form factor. In Eq. (17) the anomalous VDM transition vertex $M^{\mu}_{\gamma\gamma^*\to P}$ is given by Eq. (11). At forward angles the contribution of the tensor term $\propto F_2^p$ is marginal and can be readily neglected. The parametrization of F_1^p used here is given in [40] and follows the results of [44]. However, one could safely take $F_1^p = 1$ without much impact on the results.

The strong amplitude which describes the photoproduction of pseudoscalar mesons off nucleons by exchange of vector mesons is given by

$$-iT^{V}_{\gamma N\to PN} = -iG_{VNN}\, M^{\mu}_{\gamma V^*\to P}\, D^{V}_{\mu\nu}(l) \times \bar{u}_{s'}(p')\left[\gamma^{\nu} - \kappa_V\frac{i\sigma^{\nu\sigma}l_{\sigma}}{2m_N}\right]u_s(p). \quad (19)$$

Here $M^{\mu}_{\gamma V^*\to P}$ is given by Eq. (16) and $D^{V}_{\mu\nu}$ denotes the Feynman propagator of a V-meson

$$iD^{V}_{\mu\nu}(l) = \left[-g_{\mu\nu} + \frac{l_{\mu}l_{\nu}}{m_V^2}\right]\frac{i}{l^2 - m_V^2 + i0^+}. \quad (20)$$

The interactions of the singlet V_0^{μ} and of the octet V_8^{μ} of vector mesons with baryons (octet) B are of the form

$$v_F\langle\bar{B}\gamma_{\mu}[V_8^{\mu}, B]\rangle + v_D\langle\bar{B}\gamma_{\mu}\{V_8^{\mu}, B\}\rangle + v_S\langle\bar{B}\gamma_{\mu}B\rangle V_0^{\mu}, \quad (21)$$

where [..]({..}) commutes (anticommutes) SU(3) flavor states. Imposing the OZI rule and an ideal mixture between the singlet and the $I = 0$ of the octet one gets $v_S = \sqrt{\frac{2}{3}}(3v_F - v_D)$. Then all the other coupling constants are expressed in terms of F and D coupling constants. The couplings of the ρ^0 and ω to nucleons are given by $G_{\rho} = G_{\rho pp} = v_F + v_D$ and $G_{\omega} = G_{\omega pp} = G_{\omega nn} = 3v_F - v_D$, respectively. For the tensor VNN coupling one uses a similar flavor structure with similar F/D relations between constants. The ρNN coupling is isovector, $G_{\rho nn} = -G_{\rho pp}$, and is approximately universal [40,43], that is $G_{\rho} \simeq g/2$, where g enters the VDM equations. Therefore, we assume the same value of g in the ρNN and in the $\gamma\rho(\omega)P$ vertices. The flavor symmetry does not correlate the ωNN and ρNN couplings and we use G_{ω} as a fit parameter. The anomalous ρNN coupling is $\kappa_{\rho} = 6.1$ as in the charged pion photoproduction [40,43]. The ωNN tensor coupling is known to be very small $\kappa_{\omega} \simeq 0$.

In the photoproduction amplitude we have the contributions from the γ and from the ρ and ω exchanges

$$T_{\gamma N\to PN} = \sum_{m=\gamma,\omega,\rho} T^{m}_{\gamma N\to PN}. \quad (22)$$

However, at high energies a single pole approximation to the meson-exchange currents is not sufficient; the corresponding Feynman diagrams diverge. To regulate the high energy behavior we account for the higher mass (spin) excitations of exchanged vector mesons using the Regge propagator ($D^{V}_{\mu\nu} \to R^{V}_{\mu\nu}$)

$$iR^{V}_{\mu\nu}(l) = i\left(-g_{\mu\nu} + \frac{l_{\mu}l_{\nu}}{m_V^2}\right)\left[\frac{1 - e^{-i\pi\alpha_V(l^2)}}{2}\right] \times (-\alpha'_V)\Gamma[1 - \alpha_V(l^2)]e^{\ln(\alpha'_V s)(\alpha_V(l^2)-1)}, \quad (23)$$

where $s = (p + q)^2$ and α_V is the Regge trajectory of vector mesons

$$\alpha_V(l^2) = \alpha_V^0 + \alpha'_V l^2. \quad (24)$$

The Γ function in Eq. (23) contains the pole propagator $\sim 1/\sin(\pi\alpha_V(l^2))$ but no zeros and the amplitude's zeros only occur through the factor $1 - e^{-i\pi\alpha_V(l^2)}$. In the limit $l^2 \to m_V^2$ Eq. (23) is reduced to the standard Feynman propagator, Eq. (20). For the ω trajectory we use $\alpha_{\omega}^0 = 0.4$ and $\alpha'_{\omega} = 0.85\ \mathrm{GeV}^{-2}$ from the fit to forward and off-forward π^0 data [41]. The Regge trajectory of ρ is described by $\alpha_{\rho}^0 = 0.53$ and $\alpha'_{\rho} = 0.85\ \mathrm{GeV}^{-2}$ as in the $\pi^{\pm}$ electroproduction [40].

The results for $d\sigma/dt$ in the reaction $p(\gamma, \pi^0)p$ at forward center of mass scattering angles θ^* are shown in Fig. 2. The experimental data are from Ref. [45] and correspond to the energies of incoming photons $\nu = 3, 4, 5$, and 5.8 GeV in the laboratory. In these calculations we used the value of $G_{\omega} = 19$. Note that in the fit of low energy NN models the coupling G_{ω} is smaller $10 < G_{\omega}^2/4\pi < 20$ [46]. However, the latter values are always tied to the additional ω-nucleon form factors which are replaced here by the Reggeized propagators. Our choice of G_{ω} is necessarily not the optimal one since it also depends on the parameters of the ω-Regge trajectory used here. The solid curves in Fig. 2 describe the model results with the Primakoff (γ) and Regge (ω, ρ) exchange contributions. The strong rise of the cross section at extreme forward angles is due to the Coulomb component (Primakoff effect). In the Regge-exchange part (dashed curves) the dominant contribution comes from the ω-exchange. The dash-dotted curves describe the results without the ρ-Regge exchange.

The results for $d\sigma/dt$ in the η photoproduction off protons are shown in Fig. 3. Here the model calculations (solid curves) at $\nu = 4$ and 6 GeV are compared with forward data from Ref. [47]. The dashed curves describe the Regge-exchange contributions. In the reaction (γ, η) off nucleons the exchange of the ρ-Regge trajectory dominates the reaction mechanism.

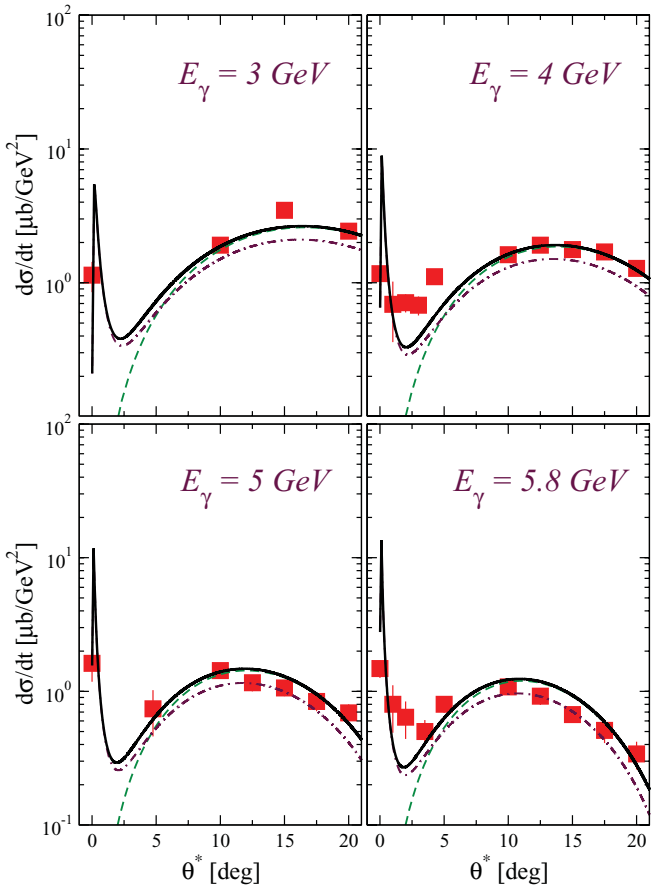

FIG. 2. (Color online) Differential cross section $d\sigma/dt$ as a function of the center of mass scattering angle θ^* in the reaction $p(\gamma, \pi^0)p$. The solid curves describe the model results with Primakoff and Regge exchange contributions. The dashed curves are the Regge exchange contributions. The dash-dotted curves describe the cross section without the ρ-exchange. The experimental data are from Ref. [45].

Furthermore, the VDM coupling g and $\eta - \eta'$ mixing angle ϑ essentially determine the magnitude of the cross section. The same mixing angle enters the Coulomb part of the amplitude and therefore determines the $\Gamma_{\eta\to\gamma\gamma}$ decay width. As one can see, at these energies the Primakoff effect in (γ, η) is barely visible on top of the large hadronic background. The available high energy (γ, η) data off protons do not allow any reliable extraction of $\Gamma_{\eta\to\gamma\gamma}$ at forward angles.

However, in the coherent production off nuclei the isovector ρ-exchange is filtered out, *i.e.* in nuclei the ρ-induced $\gamma \to \eta$ conversion off neutrons adds up destructively to the production off protons. Therefore, being effective in the elementary production off nucleons the ρ-exchange gets largely reduced in coherent reactions off nuclei due to isospin filtering. The dash-dotted curves in Fig. 3 describe the model calculations with γ and ω exchange contributions only. In this case the Primakoff peak gets much more pronounced on top of the ω-exchange background. In fact, this is a situation which is realized in the nuclear coherent production of η mesons.

The Primakoff effect in the photoproduction of η' off protons at $\nu = 6$ and 8 GeV in the laboratory is shown in

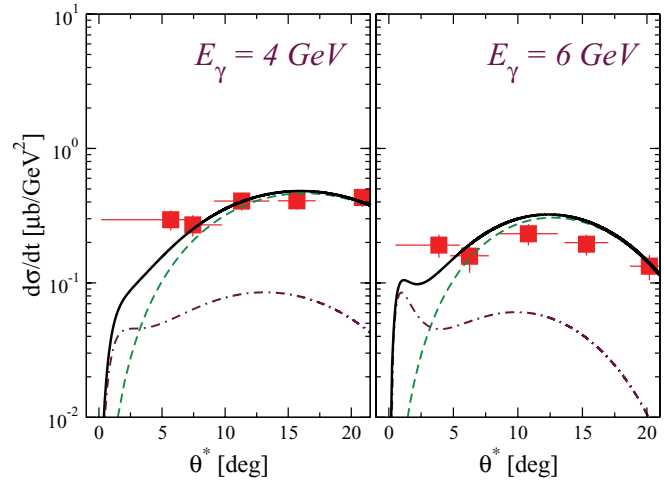

FIG. 3. (Color online) Differential cross section $d\sigma/dt$ as a function of the center of mass scattering angle θ^* in the reaction $p(\gamma, \eta)p$ at forward angles. The notations for the curves are the same as in Fig. 2. The experimental data are from Ref. [47].

Fig. 4. Here the notations for the curves are the same as in Fig. 3. As one can see, the results are qualitatively similar to the η case. The differential cross section beyond the Coulomb region is again dominated by the exchange of the ρ-Regge trajectory. Because of the higher η' mass the energy of the photons should also be much higher to separate the Primakoff component from the contribution of meson-exchange currents.

IV. COHERENT PRODUCTION OFF NUCLEI

The diagrams in Fig. 5 describe the Primakoff effect and the ω and ρ exchange contributions in the coherent π^0, η and η' photoproduction off nuclei. In the coherent reactions the residual nucleus remains in the ground state. The shaded

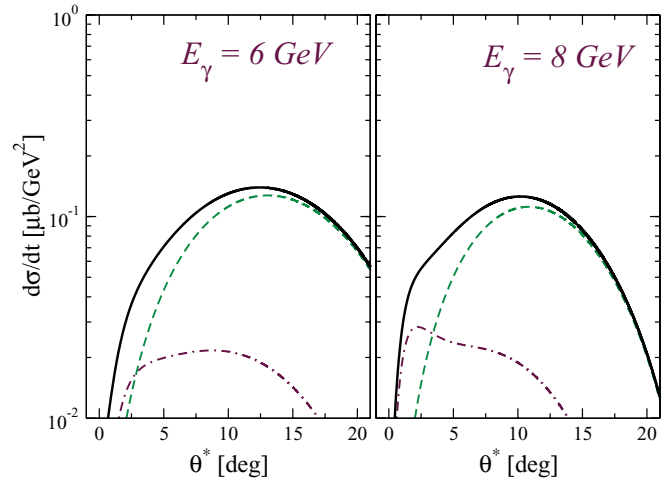

FIG. 4. (Color online) Differential cross section $d\sigma/dt$ as a function of the center of mass scattering angle θ^* in the reaction $p(\gamma, \eta')p$ at forward angles. The notations for the curves are the same as in Fig. 2.

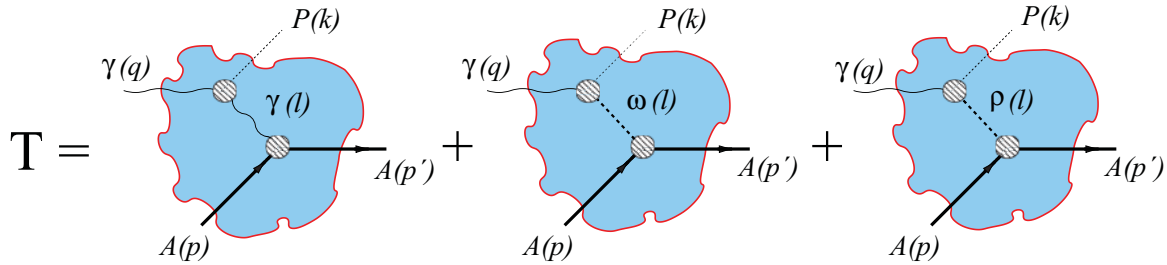

FIG. 5. (Color online) The diagrams describing the Primakoff effect (left diagram) and nuclear background ω- and ρ-Regge exchange amplitudes in high energy coherent $P = \pi^0$, η, and η' photoproduction off nuclei. The shaded regions describe a possible conversion in the nuclear medium. In this case the outgoing mesons experience FSI. The incoming photons get shadowed in ISI.

regions describe the $\gamma \to meson$ conversion in the nuclear medium. In this case the outgoing mesons experience final state interactions (FSI). The incoming photons get shadowed - initial state interactions (ISI).

The differential cross section in the reaction $\gamma(q) + A(p) \to \pi^0(k) + A(p')$ describing the bare Primakoff effect (without FSI and ISI) is given by [26,48]

$$\frac{d\sigma}{d\Omega} = \Gamma_{\pi^0\to\gamma\gamma}\frac{8\alpha Z^2}{m_\pi^3}\frac{|\vec{k}|^3\nu}{t^2}\mathcal{F}_A^2(t)\,\sin^2\theta, \tag{25}$$

where $t = (k-q)^2 = (p-p')^2$. This formula is based on the assumption that the $\gamma \to \pi^0$ conversion $\sim (\mathbf{E}\cdot\mathbf{B})$ takes place in the electric field $\mathbf{E}$ of infinitely heavy spinless $(J = 0)$ nucleus. The form factor $\mathcal{F}_A$ is related to the classical field $\mathbf{E}$ by the Fourier transform of the nuclear charge (Z) density $\rho_Z(\vec{x})$ [48].

Alternatively, one can derive Eq. (25) using a field theoretical description. Neglect again the spin of a nucleus. Then the nuclear matrix element of the nucleon vector current is

$$\begin{aligned}&-i\langle A(p')||e|\overline{\psi}\gamma^\mu\psi|A(p)\rangle\\ &\quad= -i\frac{|e|Ze^{-i(p-p')x}}{\sqrt{2E}\sqrt{2E'}}(p+p')^\mu\mathcal{F}_A(t).\end{aligned} \tag{26}$$

This is just a conserved current of a spinless state where the internal substructure is realized in the momentum space form factor $\mathcal{F}_A$. Indeed, using Eq. (26) as the γAA vertex and using the anomalous $\gamma\gamma \to \pi^0$ transition amplitude, Eq. (6), the γ-exchange Feynman diagram in Fig. 5 results (for $m_A \to \infty$) in Eq. (25).

The ωAA and ρAA interactions take essentially the same form as the γAA interaction. For instance, the ωAA interaction is obtained replacing the electromagnetic coupling $G_{\gamma A} = |e|Z$ by the strong coupling $G_{\omega A} = AG_\omega$. Note that, by this we assume that the hadronic (matter) and electromagnetic form factor distributions are essentially the same. The ω couples to the isoscalar-vector currents inside the nucleus and all the A nucleons contribute constructively to the ωA interaction.

The ρ meson couples to the isovector currents: its contribution is proportional to the difference between the number of protons and neutrons $G_{\rho A} = (2Z - A)G_\rho$ and therefore is largely suppressed. An exact ρ filtering is realized when $Z = N$. At the forward angles studied here the $\sim \kappa_\rho\sigma^{\mu\nu}$ term can be merely neglected. On the other hand, the same tensor coupling is additionally suppressed in ground state nuclei. The corresponding nuclear tensor (helicity flip) currents $-i\langle A(p')||e|\overline{\psi}\sigma^{\mu\nu}\psi|A(p)\rangle$ are marginal. This is known from the elastic electron scattering off nuclei and also from existing microscopic models for coherent π^0 and η photoproduction off nuclei [49–52].

A. General production amplitude with final state interactions

In this section we account for the fate of particles in the final state interactions. It follows that the interactions of $m = \gamma, \omega$ and ρ with a nucleus can be described by the Lagrangian

$$\begin{aligned}\mathcal{L}_{mA}(z) = &-iG_{mA}(C^\dagger(z)\partial_\mu C(z) - (\partial_\mu C^\dagger(z))C(z))\\ &\times\int d^4y F_A(y-z)\mathcal{V}_m^\mu(y),\end{aligned} \tag{27}$$

where the profile function F_A of a nucleus makes the interactions of the fields $\mathcal{V}_m^\mu$ ($\mathcal{V}_m^\mu = \mathcal{A}^\mu$, ω^μ or $\rho^{0\mu}$) non-local. F_A is normalized as follows $\int d^4y F_A(y) = 1$, where $F_A = \delta^4(y-z)$ corresponds to a point like nucleus. The Fourier transform of F_A is a form factor introduced in Eq. (26). In Eq. (27) $C^\dagger(C)$ creates (annihilates) a nucleus with $C^\dagger(z) = \int\frac{d^3\vec{k}}{\sqrt{V}}\frac{a_k^\dagger}{\sqrt{2E_k}}e^{ikz}$ with, e.g., $V = (2\pi)^3$.

Using the VDM transition vertices, see Eqs. (12) and (16), and using Eq. (27) the amplitude describing the reaction $\gamma(q,\lambda) + A(p) \to P(k) + A(p')$ is given by

$$\begin{aligned}-iT^\lambda = -i\int d^4x\int d^4y\int d^4z\int\frac{d^4l}{(2\pi)^4}F_A(y-z)\\ \times\left[\sum_{m=\gamma,\omega,\rho}d_P^{(m)}(l)\right]\varepsilon^{\mu\nu\alpha\beta}q_\mu\epsilon_\nu^\lambda l_\alpha(p+p')_\beta\\ \times e^{-i(p-p')z}e^{-il(x-y)}e^{-i(q-k)x}\chi_P^{(-)*}(\vec{x}-\vec{z}).\end{aligned} \tag{28}$$

Here $d_P^{(m)}(l)$ absorbs the propagator functions and coupling constants defined as

$$d_P^{(\gamma)}(l) = \frac{|e|}{\pi f_\pi}\frac{\alpha Z}{l^2+i0^+}F_{\gamma\gamma^*}^P(l^2), \tag{29}$$

$$\begin{aligned}d_P^{(\omega)}(l) = |e|AG_\omega G_{\gamma\omega P}\left[\frac{1-e^{-i\pi\alpha_\omega(l^2)}}{2}\right]\\ \times(-\alpha'_\omega)\Gamma[1-\alpha_\omega(l^2)]e^{\ln(\alpha'_\omega\bar{s})(\alpha_\omega(l^2)-1)},\end{aligned} \tag{30}$$

$$d_P^{(\rho)}(l) = |e|(2Z-A)G_\rho G_{\gamma\rho P}\left[\frac{1-e^{-i\pi\alpha_\rho(l^2)}}{2}\right] \times(-\alpha'_\rho)\Gamma[1-\alpha_\rho(l^2)]e^{\ln(\alpha'_\rho\bar{s})(\alpha_\rho(l^2)-1)}, \quad (31)$$

for γ, ω and ρ exchange currents, respectively. The VDM form factors $F^P_{\gamma\gamma^*}$ in Eq. (29) are defined in (12)–(14). Since ν is much bigger than the average Fermi momentum of nucleons one can take $\bar{s} = m_N^2 + 2\nu m_N$ in Eqs. (30) and (31).

Suppose, the $\gamma\gamma \to P$ or $\gamma V \to P$ conversions occur inside the nucleus. Then the outgoing meson wave acquires an additional eikonal phase $\chi_P^{(-)*}$, see Eq. (47) bellow, due to FSI. Making use of the distorted wave approximation the meson wave function in Eq. (28) reads

$$\varphi_P^{(-)*} = e^{ikx}\chi_P^{(-)*}. \quad (32)$$

In a plane wave approximation $\chi_P^{(-)*} = 1$.

At first, in Eq. (28) one has to integrate out the variable z which describes the center of mass motion of a nucleus. Introduce new variables $\xi = y - z$ and $\zeta = x - z$ with $d^4x d^4y d^4z = d^4\xi d^4\zeta d^4z$. Then one gets

$$-iT^\lambda = -i\int d^4z e^{-i(p-p'+q-k)z}\int\frac{d^4l}{(2\pi)^4}\left[\sum_{m=\gamma,\omega,\rho} d_P^{(m)}(l)\right] \times\varepsilon^{\mu\nu\alpha\beta}q_\mu\epsilon_\nu^\lambda l_\alpha(p+p')_\beta\int d^4\xi e^{il\xi}F_A(\xi) \times\int d^4\zeta e^{-i(l-k+q)\zeta}\chi_P^{(-)*}(\vec{\zeta}), \quad (33)$$

where $\int d^4z e^{-i(p-p'+q-k)z} = (2\pi)^4\delta^4(p-p'+q-k)$ describes the four-momentum conservation in the reaction. The Fourier integral $\int d^4\xi e^{il\xi}F_A(\xi) = \mathcal{F}_A(l)$ describes the nuclear form factor in the momentum space, see Eq. (26). By this Eq. (33) takes the form

$$-iT^\lambda = -i(2\pi)^4\delta^4(p-p'+q-k) \times\int\frac{d^4l}{(2\pi)^4}\left[\sum_{m=\gamma,\omega,\rho} d_P^{(m)}(l)\right]\mathcal{F}_A(l) \times\varepsilon^{\mu\nu\alpha\beta}q_\mu\epsilon_\nu^\lambda l_\alpha(p+p')_\beta\int d^4\zeta e^{-i(l-k+q)\zeta}\chi_P^{(-)*}(\vec{\zeta}). \quad (34)$$

The differential cross section is given by

$$d\sigma = \lim_{t,V\to\infty}\frac{1}{tV}\frac{\frac{1}{2}\sum_\lambda(T^\lambda T^{\lambda\dagger})}{v(2E)(2E')(2\nu)(2\omega)}\frac{d^3\vec{k}}{(2\pi)^3}\frac{d^3\vec{p}\,'}{(2\pi)^3}, \quad (35)$$

where t(time), V(volume) $\to\infty$, v is a relative γA velocity. In the laboratory, that is in the system in which the nucleus is at rest, $v = 1$. The square of the δ^4 functions in $T^\lambda T^{\lambda\dagger}$ reads $[(2\pi)^4\delta^4(p-p'+q-k)]^2 = tV(2\pi)^4\delta^4(p-p'+q-k)$ where $p = (E,\vec{p})$, $p' = (E',\vec{p}\,')$, $q = (\nu,\vec{q})$, and $k = (\omega,\vec{k})$.

In the forward kinematics studied here the mass of the nucleus is considerably larger than the recoiling momentum of the residual nucleus, i.e., $E' \to m_A$ and in the laboratory $\delta(E-E'+\nu-\omega) \to \delta(\nu-\omega)$. Then the differential cross section integrated over the three momentum of the residual nucleus and the energy ω of the outgoing meson takes the form

$$\frac{d\sigma}{d\Omega} = \frac{1}{32\pi^2}\frac{|\vec{k}|}{\nu}\sum_\lambda(M^\lambda M^{\lambda\dagger}). \quad (36)$$

Here the reduced matrix element M^λ is given by

$$M^\lambda = \int\frac{d^4l}{(2\pi)^4}\left[\sum_{m=\gamma,\omega,\rho} d_P^{(m)}(l)\right]\mathcal{F}_A(l) \times\varepsilon^{\mu\nu\alpha\beta}q_\mu\epsilon_\nu^\lambda l_\alpha n_\beta\int d^4\zeta e^{-i(l-k+q)\zeta}\chi_P^{(-)*}(\vec{\zeta}), \quad (37)$$

where

$$n = (1,0,0,0) \simeq \frac{(p+p')}{\sqrt{2E}\sqrt{2E'}} \quad (38)$$

reflects the static approximation for the target nucleus in the laboratory. It is advantageous to divide Eq. (37) into two parts

$$M^\lambda = M^\lambda_{(1)} + M^\lambda_{(2)}, \quad (39)$$

using

$$\int d^4\zeta e^{-i(l-k+q)\zeta}(1+[\chi_P^{(-)*}(\vec{\zeta})-1]). \quad (40)$$

The first term here describes a plane wave approximation (PWA). Using $\int d^4\zeta e^{-i(l-k+q)\zeta} = (2\pi)^4\delta^4(l-k+q)$ the plain wave amplitude takes the from

$$M^\lambda_{(1)} = \left[\sum_{m=\gamma,\omega,\rho} d_P^{(m)}(\vec{k}-\vec{q})\right]\mathcal{F}_A(\vec{k}-\vec{q})([\vec{k}\times\vec{q}]\cdot\vec{\epsilon}^\lambda). \quad (41)$$

If we ignore in Eq. (41) the $\omega(\rho)$-exchange contributions then one gets for $\frac{d\sigma}{d\Omega}$ a Primakoff formula, see Eq. (25).

The distorted part $M^\lambda_{(2)}$ takes into account the FSI of outgoing mesons. It is given by

$$M^\lambda_{(2)} = \int\frac{d^3\vec{l}}{(2\pi)^3}\left[\sum_{m=\gamma,\omega,\rho} d_P^{(m)}(\vec{l})\right]\mathcal{F}_A(\vec{l})([\vec{l}\times\vec{q}]\cdot\vec{\epsilon}^\lambda) \times\int d^3\vec{\zeta}\, e^{i(\vec{l}-\vec{k}+\vec{q})\vec{\zeta}}[\chi_P^{(-)*}(\vec{\zeta})-1]. \quad (42)$$

For the numerical calculations one can further simplify the distorted amplitude using the underlying spatial symmetry of the problem. Changing the order of integrations

$$M^\lambda_{(2)} = \int d^3\vec{\zeta}\, e^{-i(\vec{k}-\vec{q})\vec{\zeta}} \times\left(\left[\frac{1}{i}\vec{\nabla}_\zeta V(\vec{\zeta})\times\vec{q}\right]\cdot\vec{\epsilon}^\lambda\right)[\chi_P^{(-)*}(\vec{\zeta})-1], \quad (43)$$

where

$$V(\vec{\zeta}) = \int\frac{d^3\vec{l}}{(2\pi)^3}\left[\sum_{m=\gamma,\omega,\rho} d_P^{(m)}(\vec{l})\right]\mathcal{F}_A(\vec{l})\,e^{i\vec{l}\vec{\zeta}}. \quad (44)$$

Since, $V(\vec{\zeta}) = V(|\vec{\zeta}|)$ is spherically symmetric its divergence can be written as

$$\vec{\nabla}_\zeta V(\vec{\zeta}) = \hat{\zeta}\frac{\partial V(|\vec{\zeta}|)}{\partial|\vec{\zeta}|}, \quad (45)$$

where $\hat{\zeta}$ is a unit three vector in the direction of $\vec{\zeta}$. The resulting amplitude is a spatial integral of the form

$$M^{\lambda}_{(2)} = \int d^3\vec{\zeta}\, e^{-i(\vec{k}-\vec{q})\vec{\zeta}} \times \left(\left[\frac{1}{i}\hat{\zeta}\times\vec{q}\,\right]\cdot\vec{\epsilon}^{\,\lambda}\right)[\chi_P^{(-)*}(\vec{\zeta}\,)-1]\frac{\partial V(|\vec{\zeta}\,|)}{\partial|\vec{\zeta}\,|}. \quad (46)$$

At high energies the distortion factor is well described by the eikonal form with

$$\chi_P^{(-)*}(\vec{\zeta}\,) = e^{-\frac{1}{2}\sigma_P\int_{z_\zeta}^{\infty}\rho_A(\vec{\zeta}_\perp,\hat{k}z')dz'}, \quad (47)$$

where $\hat{k}$ is a unit three vector in the direction of outgoing meson, σ_P stands for the PN total cross section and ρ_A denotes the nuclear density, $\int d^3\vec{\zeta}\,\rho_A(\vec{\zeta}\,) = A$.

At extreme forward angles studied here the dependence on $\hat{k}$ in Eq. (47) can be readily neglected and the z' integration runs along the beam axis. In this case the azimuthal angle in Eq. (46) can be further integrated out analytically. The final result is given by the following expression ($\delta = |\vec{l}\,|$, $b = |\vec{\zeta}_\perp|$ and $z = \zeta_z$):

$$M^{\lambda}_{(2)} = ([\vec{k}\times\vec{q}\,]\cdot\vec{\epsilon}^{\,\lambda})\int_{-\infty}^{\infty}dz\int_0^{\infty}db\frac{2\pi b^2}{\sqrt{b^2+z^2}} \times e^{-i(|\vec{k}|\cos\theta-\nu)z}\frac{J_1(|\vec{k}|b\sin\theta)}{|\vec{k}|\sin\theta}[\chi_P^{(-)*}(b,z)-1] \times\int_0^{\infty}\frac{d\delta\delta^3}{2\pi^2}\left[\sum_{m=\gamma,\omega,\rho}d_P^{(m)}(\delta)\right]\mathcal{F}_A(\delta)\, j_1(\delta\sqrt{b^2+z^2}). \quad (48)$$

Here J_1 denotes the (cylindrical) Bessel function of the first kind, j_1 is the spherical Bessel function, $|\vec{k}|\cos\theta-\nu$ and $|\vec{k}|\sin\theta$ describe, respectively, the longitudinal and transverse momentum transfers to the nucleus. We note that Eqs. (41) and (48) contain both the Primakoff amplitude and the nuclear coherent amplitude as special cases.

B. Initial state interactions

In a VDM followed here the γ converts into the virtual vector mesons $V = \rho^0, \omega$ and ϕ. According to the uncertainty principle, these can further fluctuate into real state which then may rescatter coherently inside the nucleus before the production point. In this case the eikonal wave function of a photon is given by [29,53]

$$\Phi_\gamma^{(+)}(\zeta) = e^{-i\nu t}\varphi_\gamma^{(+)}(\vec{\zeta}\,) = e^{-iq\zeta}(1-S_V(\vec{\zeta}\,)), \quad (49)$$

where $S_V(\vec{\zeta}\,)$ denotes the shadowing term ($\vec{\zeta} = (\vec{\zeta}_\perp, z)$)

$$S_V(\vec{\zeta}) = \int_{-\infty}^{z}dz_i\,\rho_A(\vec{\zeta}_\perp,z_i)\frac{\sigma_V}{2}(1-i\beta_V)e^{iq_V(z_i-z)} \times e^{-\frac{\sigma_V}{2}(1-i\beta_V)\int_{z_i}^{z}dz_j\rho_A(\vec{\zeta}_\perp,z_j)}. \quad (50)$$

Here the distance l_V that the photon travels as a hadron is defined as $l_V = |q_V^{-1}|$ where $q_V = \nu - \sqrt{\nu^2 - m_V^2}$. For the average photon energy $\nu \simeq 5.2$ GeV in the PRIMEX experiment [20] the coherence length, e.g., $V = \rho^0(770)$, is $l_\rho \simeq 3.5$ fm. This value is well within the dimension of a nucleus and is just the in-medium mean free path of ρ. Therefore, we expect sizable shadowing corrections at JLAB. In Eq. (50) different VDM components shadow according to the corresponding V-nucleon cross sections σ_V and $\beta_V = \mathrm{Re}\,f_V(0)/\mathrm{Im}\,f_V(0)$ where $\mathrm{Re}\,f_V(0)(\mathrm{Im}\,f_V(0))$ describes the real (imaginary) part of the forward $VN \to VN$ scattering amplitude $f_V(0)$.

The anomalous VDM interactions involve the derivatives of vector fields, see Eq. (3). Therefore, in the shadowed amplitude one has to keep the derivative of the incoming distorted wave

$$M^{\lambda} \propto [\vec{l}\times\vec{\nabla}\varphi_\gamma^{(+)}]\cdot\vec{\epsilon}^{\,\lambda} = \varepsilon_{ijk}\epsilon_i^{\lambda}l_j\partial_k\varphi_\gamma^{(+)}, \quad (51)$$

where $\vec{\nabla}\varphi_\gamma^{(+)}$ picks up the components (ε_{ijk} is antisymmetric) which do not lie along the vector $\vec{l}$, i.e., $k \neq j$. The electromagnetic current conservation imposes further constraints on the derivative in Eq. (51). The amplitude, Eq. (37), can be written as $M^{\lambda} = \mathcal{J}^{\nu}\epsilon_{\nu}^{\lambda}$ where by gauge invariance the current $\mathcal{J}^{\nu}$ is conserved $\mathcal{J}^{\nu}q_{\nu} = 0$. In the static limit, see Eq. (38), the time component $\mathcal{J}^0 = 0$. Therefore, the product of the vector part of the current and $\vec{q}$ should give

$$[\vec{l}\times\vec{\nabla}\varphi_\gamma^{(+)}]\cdot\vec{q} = \varepsilon_{ijk}q_il_j\partial_k\varphi_\gamma^{(+)} = 0. \quad (52)$$

Because of Eq. (51), this is satisfied when $\vec{\nabla}\varphi_\gamma^{(+)}$ picks up a term which is parallel to $\vec{q} = (0,0,\nu)$. Thus, in the derivative we need the longitudinal part $\partial_z\varphi_\gamma^{(+)}$ only.

The distortion factor of a photon $\chi_V^{(+)}$ takes the form

$$\chi_V^{(+)}(\vec{\zeta}\,) = \left[1+i\frac{\sigma_V}{2\nu}(1-i\beta_V)\rho_A(\vec{\zeta}\,)\right](1-S_V(\vec{\zeta}\,)) + \frac{q_V}{\nu}S_V(\vec{\zeta}\,). \quad (53)$$

In the strong production of π^0, η, and η' only $V = \rho^0$ and ω matter. Recall that by strict OZI rule we neglected the exchange of ϕ. From the fit to data $\sigma_\rho \simeq \sigma_\omega$ [29] and the common shadowing factor factorizes in the production point. In the Primakoff production of η and η' we have an additional ϕ component. However, the strength of the $\gamma\gamma^* \to \phi\gamma^* \to \eta(\eta')$ transition is much smaller than the conversions induced by the ρ^0 intermediate state. Although, $\sigma_\phi < \sigma_\rho(\sigma_\omega)$, without much impact on the results we may assume $\sigma_\rho \simeq \sigma_\omega \simeq \sigma_\phi$ and further use the same shadowing corrections for all $\gamma - V$ transitions.

Then the distorted part of the amplitude which takes into account both the shadowing and meson FSI reads

$$M^{\lambda}_{(2)} = \int\frac{d^3\vec{l}}{(2\pi)^3}\left[\sum_{m=\gamma,\omega,\rho}d_P^{(m)}(\vec{l}\,)\right]\mathcal{F}_A(\vec{l}\,)([\vec{l}\times\vec{q}\,]\cdot\vec{\epsilon}^{\,\lambda}) \times\int d^3\vec{\zeta}\, e^{i(\vec{l}-\vec{k}+\vec{q})\vec{\zeta}}\,[\chi_P^{(-)*}(\vec{\zeta}\,)\chi_V^{(+)}(\vec{\zeta}\,)-1]. \quad (54)$$

Using the same steps as before one arrives at an expression similar to Eq. (48) with the replacement

$$[\chi_P^{(-)*}(b,z)-1] \to [\chi_P^{(-)*}(b,z)\chi_V^{(+)}(b,z)-1]. \quad (55)$$

V. RESULTS

In this section we compare the model results with π^0 photoproduction data measured at JLAB [20]. Then we extend the results to the η and η' channels. At first, we specify the input for the nuclear form factors and meson-nucleon cross sections in FSI and ISI.

The nuclear form factors entering the amplitudes are defined as follows:

$$\mathcal{F}_A(|\vec{l}\,|) = \frac{1}{Z}\int d^4x e^{ilx}\delta(x_0)\rho_Z(\vec{x}) = \frac{4\pi}{Z}\int d|\vec{x}\,|\,|\vec{x}\,|^2 j_0(|\vec{l}\,||\vec{x}\,|)\rho_Z(|\vec{x}|), \quad (56)$$

where the charge density distributions $\rho_Z(\vec{x}) = \rho_Z(|\vec{x}|)$ of nuclei are parametrized according to Ref. [54]. For the matter density distributions we assume $\rho_A(\vec{x}) = \frac{A}{Z}\rho_Z(\vec{x})$.

The ρ^0-nucleon cross section $\sigma_V = \sigma_\rho$ and $\beta_V = \beta_\rho$ in Eqs. (50) and (53) are taken from [29]. By isospin the total $\pi^0 N$ cross section in Eq. (47) would be $\sigma_{\pi^0} = \frac{1}{2}(\sigma_{\pi^+} + \sigma_{\pi^-})$. This value is in agreement with the quark model estimate $\sigma_{\pi^0} \simeq \sigma_\rho$. For the ηN and $\eta' N$ cross sections σ_η and $\sigma_{\eta'}$, respectively, we assume the same value as $\sigma_{\pi^0}(\sigma_\rho)$. Then the only model input is $\sigma_V = \sigma_\rho$ from the fit to data by [29] where $\sigma_V = 20.8(1 + \frac{0.766}{\sqrt{\nu^2 - m_\rho^2}})$ mb and $\beta_V = \frac{0.766}{\sqrt{\nu^2 - m_\rho^2}+0.766}$.

A. π^0 photoproduction at JLAB

High precision measurements of the differential cross sections $d\sigma/d\theta$ in π^0 photoproduction off nuclei at forward angles have been performed in the PRIMEX experiment at JLAB [20] with ^{12}C and ^{208}Pb as the targets. The $\pi^0 \to \gamma\gamma$ decay width has been extracted with the magnitudes of nuclear coherent, nuclear incoherent and the phase angle between the Primakoff and the nuclear coherent amplitudes being parameters in the extraction.

At first, we consider the effects of FSI and shadowing on the Primakoff effect. In Fig. 6 we show the in-medium distortion of the Primakoff signal in the coherent production of π^0 off ^{12}C (bottom curves) and ^{208}Pb (top curves) nuclei in the kinematics of the PRIMEX experiment. The incoming photon energy in the laboratory is $\nu = 5.2$ GeV; this is an average value used at JLAB. The dashed curves describe the calculations without any in-medium interactions of incoming (γ) and outgoing (π^0) particles. The dash-dotted curves include the effect of FSI only. The solid curves include FSI of pions and photon shadowing in ISI. As one can see, the latter have practically no influence on the Coulomb peak at forward angles for both nuclei where the width $\Gamma_{\pi^0\to\gamma\gamma}$ is extracted. For ^{208}Pb the tail of the Primakoff signal at $\theta \sim 0.5^\circ$–0.75° gets largely distorted by FSI, but the magnitude of the signal is already very small there.

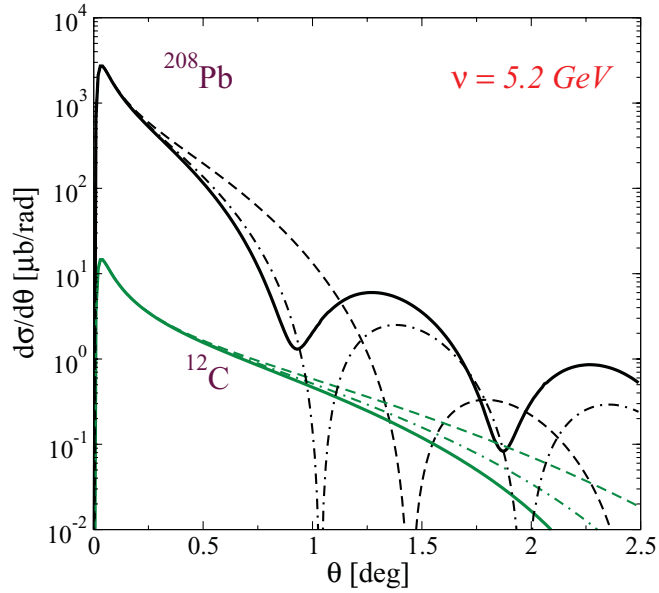

FIG. 6. (Color online) Primakoff effect in coherent photoproduction of π^0-meson off ^{12}C (bottom curves) and ^{208}Pb (top curves) nuclei in the kinematics of the PRIMEX experiment [20]. The incoming photon energy $\nu = 5.2$ GeV in the laboratory. The dashed curves describe the calculations without any in-medium interactions of incoming (γ) and outgoing (π^0) particles. The dash-dotted curves describe the effect of FSI. The solid curves include FSI and γ-shadowing in ISI.

To compare the model results with experimental data the theoretical cross sections have to be folded with the photon energy spectrum and the angular resolution. The experimental spectrum of the incident photons is essentially an uniform distribution over the tagged range of $\nu = 4.9$–5.5 GeV [55]. The angular distribution to be compared with data is

$$\frac{1}{\Delta\nu}\int_{\Delta\nu} d\nu \int d\theta_i \frac{d\sigma(\nu,\theta_i)}{d\theta_i} P(\theta,\theta_i), \quad (57)$$

where $P(\theta,\theta_i) = \frac{1}{b\sqrt{\pi}} e^{-(\theta-\theta_i)^2/b^2}$ with $b = \frac{\Delta\theta}{2\sqrt{\ln 2}}$ describes the Gaussian angular resolution with the width of $\Delta\theta = 0.4$ mrad [56].

In Fig. 7 the experimental differential cross section [20] $d\sigma/d\theta$ in the reaction (γ,π^0) off ^{208}Pb is compared with our model results. The data exhibit the sharp forward peak characteristic of Primakoff production. The weaker dependence at larger θ is due to strong coherent π^0 production.[2] The incoherent cross section for a ^{208}Pb target (not shown here) is tiny at these small angles and thus makes no significant contribution in the region of the Primakoff signal [20]. The solid curves in the left and right panels of Fig. 7 are our model results for the total coherent cross section. The Primakoff (γ) and the nuclear coherent Regge ω and ρ exchange contributions together with FSI and ISI are taken into account. In the left panel the dash-dotted curve describes the model

[2]Note that the experimental spectrum contains both the coherent and incoherent cross sections.

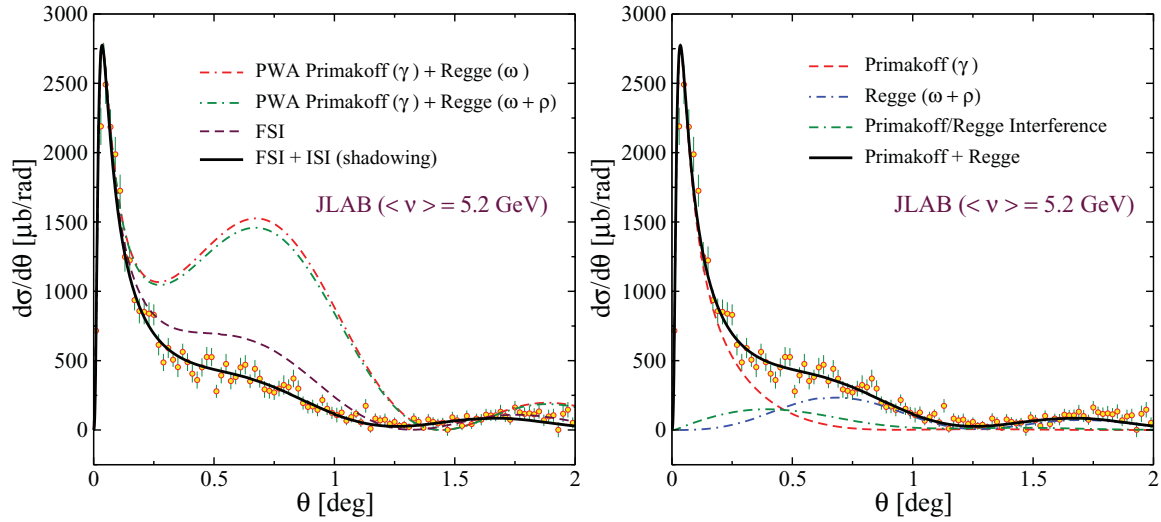

FIG. 7. (Color online) Differential cross section $d\sigma/d\theta$ in the reaction (γ, π^0) off ^{208}Pb target as a function of π^0 production angle θ in the laboratory. The experimental data are from Ref. [20]. The solid curves in the left and right panels describe the model coherent cross section with meson FSI and photon shadowing in ISI with the average value of $\nu = 5.2$ GeV. The Primakoff (γ) and nuclear coherent (Regge ($\omega + \rho$) exchange) contributions are taken into account. Left panel: The dash-dotted curve describe the model results in a plain wave approximation. The dash-dash-dotted curve corresponds to the plain wave approximation (PWA) without the exchange of ρ-Regge trajectory. The dashed curve accounts for the effect of FSI only. Right panel: The dashed and dash-dotted curves describe the nuclear coherent Primakoff and Regge ($\omega + \rho$) exchange contributions, respectively. The dash-dash-dotted curve describes the interference between the Primakoff and Regge exchange contributions.

results in a PWA. Also the dash-dash-dotted curve describes the plain wave results without the exchange of the ρ-meson Regge trajectory. Because of the large excess of neutrons over the number of protons in ^{208}Pb the ρ-exchange contributes destructively in this case. The bump between $\theta \sim 0.5^\circ$–1° is due to nuclear coherent production. It gets strongly reduced by FSI of the produced pions. In the left panel the dashed curve accounts for FSI of pions without shadowing in ISI.

In the right panel of Fig. 7 we show different reaction mechanisms which contribute to the cross section. The dashed curve is the Primakoff effect. The dash-dotted curve describe the Regge exchange contributions, labeled as nuclear coherent in Ref. [20]. The dash-dash-dotted curve describes the interference between the Primakoff and Regge exchange amplitudes.

In Fig. 8 we compare the model results with the measured differential cross sections $d\sigma/d\theta$ in the π^0 photoproduction off ^{12}C nucleus. The notations for the curves in both panels are the same as in Fig. 7. In the production of ^{12}C the isospin filtering is realized exactly. Therefore, there is no ρ-exchange

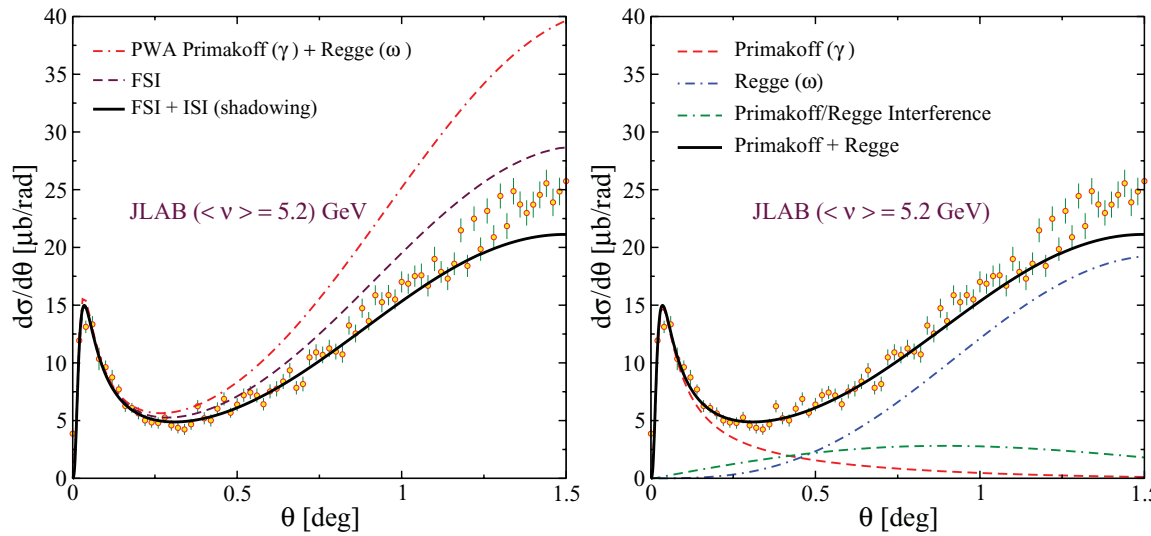

FIG. 8. (Color online) Differential cross section $d\sigma/d\theta$ in the reaction (γ, π^0) off ^{12}C target as a function of π^0 production angle θ in the laboratory. The experimental data are from Ref. [20]. The notations for the curves in both panels are the same as in Fig. 7.

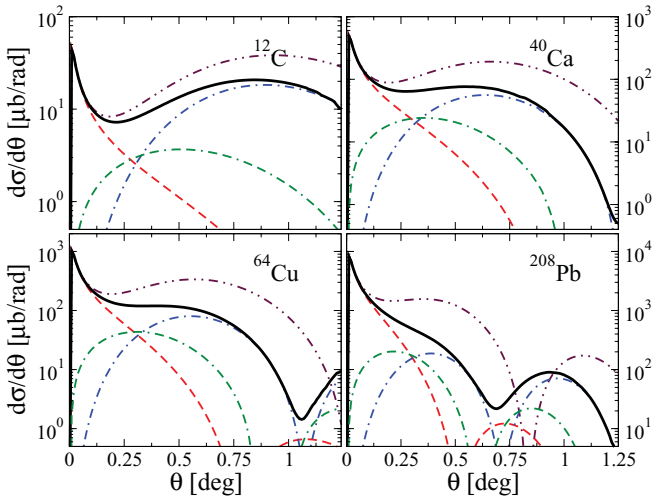

FIG. 9. (Color online) Differential cross section $d\sigma/d\theta$ in the reaction $A(\gamma,\pi^0)A$ off ^{12}C, ^{40}Ca, ^{64}Cu, and ^{208}Pb nuclei. The incoming photon energy in the laboratory is $\nu = 9$ GeV. The solid curves describe the model results. The dashed, dash-dotted and dash-dash-dotted curves describe the Primakoff, Regge and interference Primakoff/Regge cross sections, respectively. The dot-dot-dashed curves correspond to the PWA.

contribution in this case. The nuclear coherent background (dashed curve in the right panel) is dominated by the exchange of the ω-Regge trajectory. The model results (solid curves) are in agreement with data below $\theta \simeq 1^\circ$. For ^{12}C this is a region where the coherent Primakoff and Regge exchange contributions dominate the cross section. The incoherent cross section is largely suppressed in this region. However, it gives a sizable contribution beyond that region where the difference between the model results and data is due to the incoherent π^0 production [20].

Note that the calculation of the incoherent cross section is conceptually different. Since the nucleus breaks up (or gets excited) in this case the coherence is lost and the nuclear cross section is given by the sum of individual nucleon cross sections corrected for the effects of Fermi motion, Pauli blocking, shadowing and FSI. The FSI contain coupled channel effects, such a charge exchange, so that the final π^0 could not be the one initially produced. In line with our transport theoretical model [22] these calculations will be presented in forthcoming publications.

Summarizing these comparisons, the overall agreement of the full calculation with present data is remarkable and there is no need to introduce any further fit parameters to describe the data at forward angles. Note that contrary to the treatment in [20,28] the relative weights of the various contributions are all fixed from the elementary process so that no further adjustment to the nuclear data can be performed. We recall that in [20] the relative strengths and phases of the various amplitudes were fitted to experiment and turned out to depend even on mass number.

This agreement encourages us now to make predictions for higher energies and other mesons. The model predictions for higher energies ($\nu = 9$ GeV) are shown in Fig. 9. The solid curves describe the model results for the coherent cross section. The dashed, dash-dotted and dash-dash-dotted curves correspond to the Primakoff, Regge and interference Primakoff/Regge cross sections, respectively. The dot-dot-dashed curves correspond to the plane wave approximation. As one can see, in all cases the Primakoff peak dominates over the Regge behavior of the nuclear background. Furthermore, for heavy nuclei the Primakoff effect dominates the overall reaction mechanism.

The in-medium distortion of the Primakoff signal for pions at $\nu = 9$ GeV off ^{12}C (bottom curves) and ^{64}Cu nuclei is shown in the left panel of Fig. 10. In the middle and right panel we also present the results for the Primakoff effect in the coherent production of η and η' mesons, respectively. In Fig. 10 the dashed curves describe the bare Coulomb component in a plane wave approximation. The solid curves include FSI and shadowing corrections. As one can see, in the π^0 production (left panel) at the maximum of the Primakoff effect the

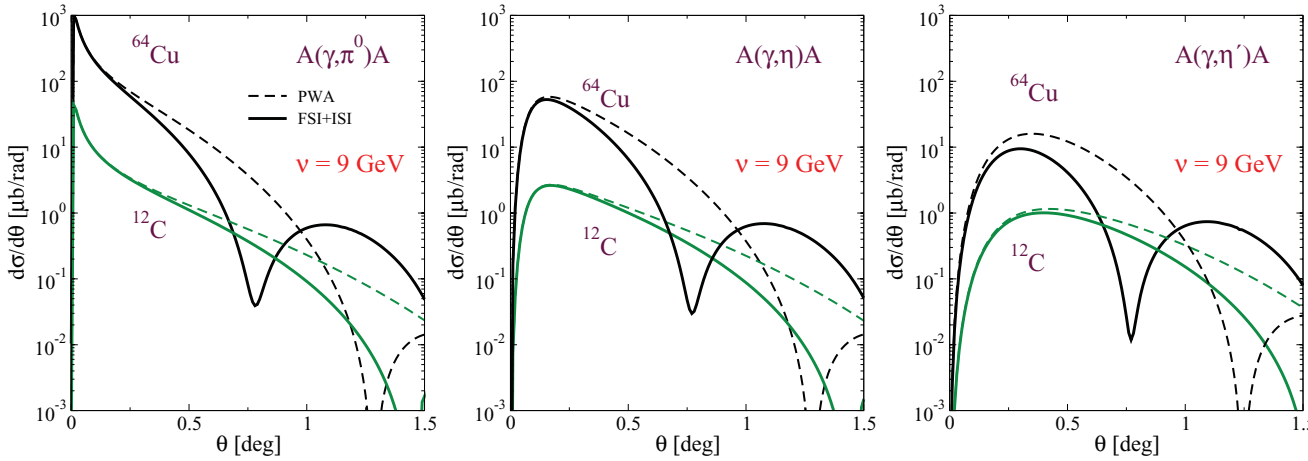

FIG. 10. (Color online) Primakoff effect in the coherent production of π^0 (left panel), η (middle panel) and η' (right panel) off ^{12}C (bottom curves) and ^{64}Cu nuclei. The calculations are performed for the photon energy $\nu = 9$ GeV in the laboratory. The solid (dashed) curves describe the calculations with (without) final and initial state interactions.

in-medium distortion of incoming and outgoing waves does not affect the $\gamma\gamma^* \to \pi^0$ signal. In the off-forward region, however, the distortion is large and changes the shape of the signal. These changes are much more pronounced for heavy systems.

In contrast, the peak positions for the η and η' signals are shifted to larger angles because at fixed photon energy the position of the Primakoff signal depends on the mass of the produced meson $\propto m_P^2/\nu$. Since the photon excitation to the heavy η and η' states requires somewhat bigger momentum transfers to the nucleus than for the pions the range of the corresponding interactions is much smaller. These conversions are then not peripheral anymore as in the π^0 case and may proceed deep inside the nucleus. As a consequence, Primakoff and nuclear coherent excitations become entangled.

B. $\eta(547)$ photoproduction off nuclei

In Fig. 11 we present our results for the η production in the kinematics accessible at present JLAB energies. The calculations correspond to the incoming photon energy $\nu = 5.2$ GeV in the laboratory. Recall that in the elementary production of nucleons the Primakoff signal is barely visible on top of the strong background. On the contrary, the filtering of the ρ-exchange makes the nuclear Primakoff effect pronounced already at these photon energies. For instance, on heavy targets the Coulomb peak dominates over the Regge exchange contributions. This makes further experimental studies of the Primakoff effect at present JLAB energies promising. The situation would be much better at higher energies.

For the measurements of the $\pi^0 \to \gamma\gamma$ and $\eta \to \gamma\gamma$ decay widths in the Primakoff effect at present JLAB energies, Fig. 12 (left panel) demonstrates the distortion of the Primakoff signal in the π^0 photoproduction off ^{208}Pb target. The distortion factor in Fig. 12 is defined as the ratio of the model and bare (without FSI and ISI) Primakoff cross sections. As one can see the distortion of the signal due to the FSI (dash-dotted), FSI+ISI (dashed), and strong production (solid) is less than

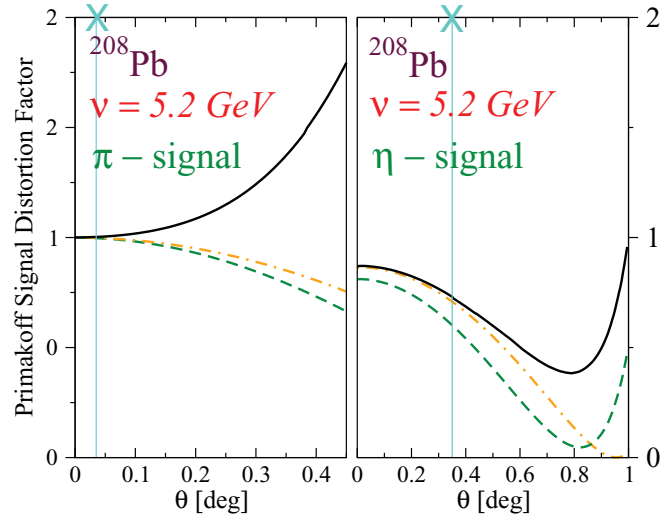

FIG. 12. (Color online) Distortion of the bare Primakoff signal at $\nu = 5.2$ GeV in the coherent reactions $^{208}\mathrm{Pb}(\gamma, \pi^0)^{208}\mathrm{Pb}$ (left panel), $^{208}\mathrm{Pb}(\gamma, \eta)^{208}\mathrm{Pb}$ (right panel) due to FSI (dash-dotted), FSI+ISI (dashed) and strong production (solid). The crossed symbol shows the position of the maximum of the Primakoff signal where the decay width is extracted.

<1% around the maximum of the Primakoff signal (crossed symbol). On the contrary, for the η (right panel in Fig. 12) the distortion is already significantly larger.

The results for the Primakoff effect in the photoproduction of η mesons at $\nu = 9$ GeV are shown in the middle panel of Fig. 10. This energy region corresponds to an approved experimental proposal for the η production via the Primakoff effect in Hall D at JLAB [21]. As one can see, the magnitude of the Coulomb signal is barely affected by FSI and ISI at forward angles in both light and heavy systems. In Fig. 13 we show the model predictions at $\nu = 9$ GeV which include both the Primakoff and Regge exchange contributions.

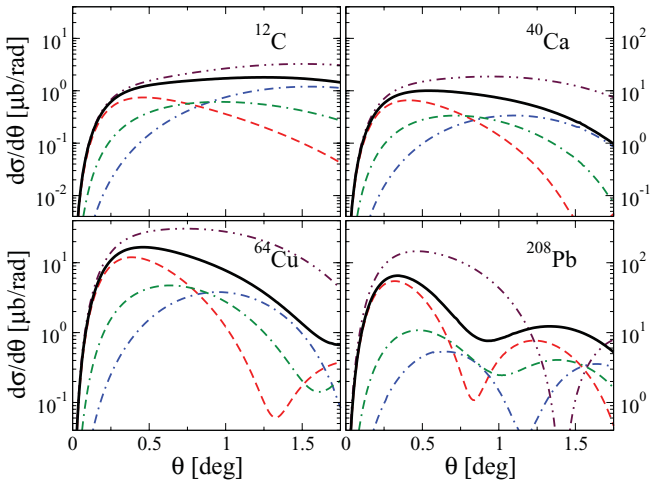

FIG. 11. (Color online) Differential cross section $d\sigma/d\theta$ in the reaction $A(\gamma, \eta)A$ at $\nu = 5.2$ GeV in the laboratory. The notations for the curves are the same as in Fig. 9.

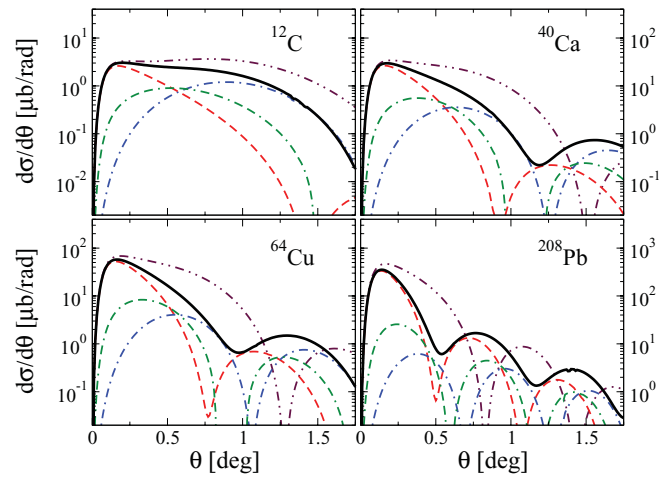

FIG. 13. (Color online) Differential cross section $d\sigma/d\theta$ in the reaction $A(\gamma, \eta)A$ at $\nu = 9$ GeV in the laboratory. The notations for the curves are the same as in Fig. 9.

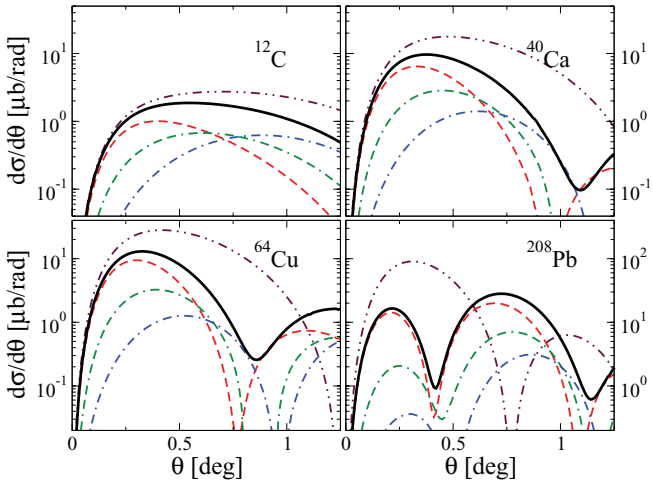

FIG. 14. (Color online) Differential cross section $d\sigma/d\theta$ in the reaction $A(\gamma, \eta')A$ at $\nu = 9$ GeV in the laboratory. The notations for the curves are the same as in Fig. 9.

C. $\eta'(958)$ photoproduction off nuclei

In Fig. 10 (right panel) the results for the Primakoff production of η' meson at $\nu = 9$ GeV are shown. This result is instructive since it suggest a use of light systems to minimize the in-medium effects in the region of the Coulomb peak. For heavy systems the signal is strongly affected by the in-medium interactions. Therefore, the use of light nuclear targets preferable. The price at these energies is smaller cross sections than in the production off heavy targets.

The coherent production of η' for $\nu = 9$ GeV are shown in Fig. 14. The notations for the curves are the same as in Fig. 9. Because of the suppression of the ρ-Regge exchange the Primakoff signal is large (dashed curves) and dominates over the nuclear coherent background (dash-dotted curves). The relative contribution of the nuclear coherent cross section is getting small with increasing mass number of a nucleus. However, the interference cross section (dash-dash-dotted curves) gets large. This feature can be seen in the η production also. Interestingly what contaminates the Primakoff signal is a large interference between the Coulomb and strong amplitudes.

VI. SUMMARY

In summary, we have considered the high energy coherent photoproduction of pseudoscalar mesons π^0, η and η' off nuclei. All the calculations presented here have been performed at extreme forward angles where the Primakoff effect is expected to dominate the nuclear photoproduction mechanism. At high energies the Primakoff signal is expected to be well separated from the nuclear background contributions. If true this allows to measure the radiative $\gamma\gamma$ decay widths of pseudoscalar mesons.

In reality the interference of the Primakoff amplitude with the nuclear coherent amplitude contaminates the signal. Furthermore, the conversion of photons to mesons deep inside the nucleus distorts the signal by FSI and photon shadowing in ISI. The data analysis and width extraction thus have to be based on a model which is able to describe the different production mechanisms reliably.

In the present work we have proposed such a model for the coherent production of mesons which treats the Coulomb and strong nuclear components in the same footing. Starting from the VDM description of the anomalous sector we have established the transition amplitudes which have been used to describe the photoproduction process off nucleons. A use of Reggeon exchanges allows to start from the description of the elementary cross sections off nucleons and take into account the complex phase between the Primakoff and Regge exchange amplitudes. In VDM both the radiative $\gamma\gamma \to P$ and $\gamma V \to P$ transitions are correlated. This allows to calculate consistently the in-medium interactions of mesons and photons in the final and initial states, respectively. Contrary to previously existing approaches our model describes simultaneously the Primakoff (γ), Regge (ω, ρ), and the interference Primakoff/Regge exchange contributions with the same input from the reactions off *nucleons*.

Furthermore, we have explicitly demonstrated the importance of FSI and shadowing corrections in ISI in the coherent π^0 photoproduction reactions of *nuclei*. The model describes the forward region around the Primakoff signal measured in the π^0 photoproduction at JLAB very well. There was no need to introduce any additional parameters to match the model cross sections with the experimental data.

The extremely small distortion of the π^0 Primakoff signal by other processes explains why the various nuclear fit parameters in the analysis of [28] do not affect the actual signal. This is very different, however, for the η and η' Primakoff experiments where the strong nuclear distortions are large in the peak region and have to be well under control. Therefore, we have also calculated cross sections for the photoproduction of η and η' mesons. We find that because of the isospin filtering of the ρ exchange the Primakoff signal in the η production off nuclei is still large compared with the nuclear coherent background already at present JLAB energies. However, at these energies there are already significant distortions due to FSI, ISI and the strong amplitude, see Fig. 12 (right panel). In the case of η and η' high energy data from future JLAB experiments may make the study of the Primakoff effect and an extraction of the $\eta(\eta') \to \gamma\gamma$ decay width possible. In both η and η' cases the coherent production provide at the same time a filter and an amplifying device which allows to isolate the Primakoff γ-exchange production mechanisms which otherwise remain hidden in the background. The observed sensitivity of the cross sections to the in-medium η and η' interactions may also provide a complementary way to measure the unknown $\eta(\eta')$-nucleon cross sections.

ACKNOWLEDGMENTS

We are grateful to A. Bernstein and A. Gasparian for helpful communications and reading the manuscript. This work was supported by DFG through TR16 and by BMBF.

APPENDIX: NOTATIONS FOR P AND V_μ MATRICES

The mixing pattern of the SU(3) singlet V_0^μ and the isospin $I = 0$ octet of vector mesons V_8^μ is supposed to be ideal, that is $\omega(782) = \sqrt{\frac{2}{3}}V_0 + \sqrt{\frac{1}{3}}V_8^{I=0}$ and $\phi(1020) = \sqrt{\frac{1}{3}}V_0 - \sqrt{\frac{2}{3}}V_8^{I=0}$. Thus, the vector mesons are described by the matrix V_μ

$$\begin{pmatrix} \rho^0 + \omega & 0 & 0 \\ 0 & -\rho^0 + \omega & 0 \\ 0 & 0 & \sqrt{2}\phi \end{pmatrix}_\mu . \tag{A1}$$

The diagonal components of the nonet of pseudoscalar mesons $P = P_8 + P_0$ are incorporated into the matrix

$$\begin{pmatrix} \pi^0 + \frac{\eta_8}{\sqrt{3}} + \sqrt{\frac{2}{3}}\eta_0 & 0 & 0 \\ 0 & -\pi^0 + \frac{\eta_8}{\sqrt{3}} + \sqrt{\frac{2}{3}}\eta_0 & 0 \\ 0 & 0 & -\frac{2\eta_8}{\sqrt{3}} + \sqrt{\frac{2}{3}}\eta_0 \end{pmatrix}, \tag{A2}$$

where $\eta_0 - \eta_8$ mixing is described in Sec. II.

[1] H. Primakoff, Phys. Rev. **81**, 899 (1951).
[2] D. Berg *et al.*, Phys. Rev. Lett. **44**, 706 (1980).
[3] T. Jensen *et al.*, Phys. Rev. D **27**, 26 (1983).
[4] J. Huston *et al.*, Phys. Rev. D **33**, 3199 (1986).
[5] L. Capraro *et al.*, Nucl. Phys. B **288**, 659 (1987).
[6] C. Bemporad *et al.*, Nucl. Phys. B **51**, 1 (1973).
[7] D. Berg *et al.*, Phys. Lett. B **98**, 119 (1981).
[8] C. Chandlee *et al.*, Phys. Rev. Lett. **51**, 168 (1983).
[9] M. Zielinski *et al.*, Phys. Rev. Lett. **52**, 1195 (1984).
[10] B. Collick *et al.*, Phys. Rev. Lett. **53**, 2374 (1984).
[11] T. Devlin, P. C. Petersen, and A. Beretvas, Phys. Rev. D **34**, 1626 (1986).
[12] P. C. Petersen *et al.*, Phys. Rev. Lett. **57**, 949 (1986).
[13] K. Zioutas *et al.*, Phys. Rev. Lett. **94**, 121301 (2005).
[14] J. S. Bell and R. Jackiw, Nuovo Cim. A **60**, 47 (1969).
[15] S. L. Adler, Phys. Rev. **177**, 2426 (1969).
[16] V. I. Kryshkin, A. G. Sterligov, and Y. P. Usov, Zh. Eksp. Teor. Fiz. **57**, 1917 (1969).
[17] A. Browman *et al.*, Phys. Rev. Lett. **33**, 1400 (1974).
[18] A. Browman *et al.*, Phys. Rev. Lett. **32**, 1067 (1974).
[19] C. Bemporad *et al.*, Phys. Lett. B **25**, 380 (1967).
[20] I. Larin *et al.*, Phys. Rev. Lett. **106**, 162303 (2011).
[21] A. Gasparian *et al.*, JLAB experiment E12-10-011, [http://www.jlab.org/exp_prog/proposals/11prop.html].
[22] M. M. Kaskulov, K. Gallmeister, and U. Mosel, Phys. Rev. C **79**, 015207 (2009).
[23] T. E. Rodrigues *et al.*, Phys. Rev. C **82**, 024608 (2010).
[24] W. Cosyn, M. C. Martinez, and J. Ryckebusch, Phys. Rev. C **77**, 034602 (2008).
[25] S. Gevorkyan *et al.*, arXiv:0908.1297 [hep-ph].
[26] G. Morpurgo, Nuovo Cimento **31**, 569 (1964).
[27] G. Fäldt, Nucl. Phys. B **43**, 591 (1972).
[28] S. Gevorkyan, A. Gasparian, L. Gan, I. Larin, and M. Khandaker, Phys. Rev. C **80**, 055201 (2009).
[29] T. H. Bauer *et al.*, Rev. Mod. Phys. **50**, 261 (1978).
[30] J. Wess and B. Zumino, Phys. Lett. B **37**, 95 (1971).
[31] E. Witten, Nucl. Phys. B **223**, 422 (1983).
[32] H. Leutwyler, Nucl. Phys. Proc. Suppl. **64**, 223 (1998).
[33] H. B. O'Connell *et al.*, Prog. Part. Nucl. Phys. **39**, 201 (1997).
[34] K. Kawarabayashi and M. Suzuki, Phys. Rev. Lett. **16**, 255 (1966); Riazuddin and Fayyazuddin, Phys. Rev. **147**, 1071 (1966).
[35] A. M. Bernstein, PoS **CD09**, 035 (2009).
[36] C. Amsler *et al.* (Particle Data Group), Phys. Lett. B **667**, 1 (2008).
[37] A. Sibirtsev *et al.*, Eur. Phys. J. A **44**, 169 (2010).
[38] A. Sibirtsev *et al.*, Eur. Phys. J. A **41**, 71 (2009).
[39] C. Terschlusen and S. Leupold, Phys. Lett. B **691**, 191 (2010).
[40] M. M. Kaskulov and U. Mosel, Phys. Rev. C **81**, 045202 (2010); arXiv:1103.1602 [nucl-th]; arXiv:1101.6042 [hep-ph].
[41] M. M. Kaskulov, arXiv:1105.1993 [nucl-th].
[42] M. M. Kaskulov, K. Gallmeister, and U. Mosel, Phys. Rev. D **78**, 114022 (2008); M. M. Kaskulov and U. Mosel, Phys. Rev. C **80**, 028202 (2009).
[43] J. M. Laget, Phys. Rev. C **72**, 022202 (2005).
[44] M. M. Kaskulov and P. Grabmayr, Phys. Rev. C **67**, 042201 (2003); **69**, 028201 (2004).
[45] M. Braunschweig *et al.*, Nucl. Phys. B **20**, 191 (1970).
[46] R. Machleidt, K. Holinde, and C. Elster, Phys. Rep. **149**, 1 (1987).
[47] W. Braunschweig *et al.*, Phys. Lett. B **33**, 236 (1970).
[48] E. Hadjimichael and S. Fallieros, Phys. Rev. C **39**, 1438 (1989).
[49] J. Piekarewicz, A. J. Sarty, and M. Benmerrouche, Phys. Rev. C **55**, 2571 (1997).
[50] W. Peters, H. Lenske, and U. Mosel, Nucl. Phys. A **642**, 506 (1998).
[51] W. Peters, H. Lenske, and U. Mosel, Nucl. Phys. A **640**, 89 (1998).
[52] M. M. Kaskulov and A. V. Bibikov, Moscow Univ. Phys. Bull. **56**, 30 (2001); V. V. Balashov, V. K. Dolinov, and M. M. Kaskulov, Eur. Phys. J. A **11**, 231 (2001).
[53] T. Falter, K. Gallmeister, and U. Mosel, Phys. Rev. C **67**, 054606 (2003).
[54] C. W. De Jager, H. De Vries, and C. De Vries, Atom. Data Nucl. Data Tabl. **14**, 479 (1974).
[55] A. Teymurazyan, Ph.D. thesis, University of Kentucky, 2008.
[56] A. Gasparian (private communication).